Taming intrinsic localized modes in a DNA lattice with damping, external force, and inhomogeneity

Carlos Lawrence Gninzanlong,[1,*] Frank Thomas Ndjomatchoua,[2,†] and Clément Tchawoua[1,‡]
[1]*Department of Physics, Faculty of Science, University of Yaoundé 1, P.O. Box 812, Yaoundé, Cameroon*
[2]*Sustainable Impact Platform, Adaptive Agronomy and Pest Ecology Cluster, International Rice Research Institute (IRRI), DAPO Box 7777-1301, Metro Manila, Philippines*

(Received 31 October 2018; revised manuscript received 10 April 2019; published 13 May 2019)

The dynamics of DNA in the presence of uniform damping and periodic force is studied. The damped and driven Joyeux-Buyukdagli model is used to investigate the formation of intrinsic localized modes (ILMs). Branches of ILMs are identified as well as their orbital stabilities. A study of the effect of inhomogeneity introduced into the DNA lattice and its ability to control chaotic behavior is conducted. It is seen that a single defect in the chain can induce synchronized spatiotemporal patterns, despite the fact that the entire set of oscillators and the impurity are chaotic when uncoupled. It is also shown that the periodic excitation applied on a specific site can drive the whole lattice into chaotic or regular spatial and temporal patterns.

DOI: 10.1103/PhysRevE.99.052210

I. INTRODUCTION

Discrete breathers also termed intrinsic localized modes (ILMs) are spatially localized, temporally periodic excitations with an exponentially localized profile in nonlinear lattices [1,2]. Because they occur in discrete systems, they have been termed discrete breathers (DBs) in reference to their continuum analogs, called breathers, which were first discovered in completely integrable and continuous nonlinear wave equations [3]. While discrete breathers share many traits with solitons, they stand out because of their localization, which is brought about by a delicate sensitivity to lattice discreteness [3]. Discrete breathers have been ubiquitously studied in a wide variety of physical systems and have been the subject of intense theoretical and numerical scrutiny [1,2]. Although dissipation and driving are typically key experimental features, most of the theoretical and numerical studies found in the literature excluded such effects. It was not until quite recently that the effects of dissipation and uniform periodic driving have been considered in numerical studies of discrete breathers in nonlinear physical systems, including (but not limited to) the Frenkel-Kontorova chain and a ladder of Josephson junctions [4,5], coupled pendulums [6–8], discrete electrical transmission lines [9–14], and a micromechanical cantilever array [15,16]. Accounting for such constraints allowed these researchers to generate and control the dynamics of DBs as well as to stabilize them [4–16].

The majority of biomolecules are assembled under the form of lattices, and they are constantly submitted to fluid frictional forces induced by biological plasmas and exposed to external periodic electromagnetic radiation. Thus they represent a worthwhile contextual framework in which a DB would certainly play an important role, and dissipation and driving cannot be ignored. The biomolecules called DNA represent a system in which localization and energy transfer emerge as prevailing regulatory factors [17]. The Peyrard-Bishop-Dauxois (PBD) model of double-stranded DNA is arguably one of the most successful models for describing this local pairing-unpairing (breathing) dynamics because it reproduces a wide variety of qualitative results closer to experiments related to strand-separation dynamics [18]. Joyeux and Buyukdagli (JB) refined this model in such a way that it can account for on-site finite stacking enthalpy [19,20]. Such a modification yielded phase-transition curves in agreement with the denaturation observed by Raman spectroscopy, and it ensured a sharp melting transition [19,20]. Therefore, the JB model is selected as the core model in this study. On the one hand, the JB model was further analyzed free of external forces and without damping in order to look for analytical semidiscrete solutions and investigate their modulational stability [21–24]. On the other hand, motivated by the fact that oscillating terahertz (THz) drive applied in DNA can generate breathing states linked to gene expression [25–28], the PBD model was modified in order to include a monochromatic drive in the THz frequency range, and it was suggested to represent a simplified model for DNA dynamics in the presence of THz radiation [29–32].

Several studies taking into account the effects of dissipation (and/or of the periodic force) were performed on the DNA models presented in Refs. [29–32], but none of these studies generated ILMs by taking into account both dissipation and periodic force. In this study, we discuss the generation of ILMs that are locked to a uniform periodic driver and dissipation based in the JB model. The emphasis is on the characterization and stability of these modes. The spatial and temporal control of the chaotic behavior, as well as the effect of inhomogeneity and an external force, are also analyzed.

*gcarloslawrence@yahoo.fr
†ftndjomatchoua@gmail.com
‡Author to whom all correspondence should be addressed: ctchawa@yahoo.fr

It is worth noting that numerous authors have studied the effect of periodic forces on DBs of nonlinear lattices without dissipative forces by separating the space and time components [33–39]. Such a modification can straightforwardly reduce the system to a single degree of freedom embedding the parameters that are suitable for the generation of a generalized shape for the DB [36], which can further be analyzed using classical methods to study nonlinear dynamical system responses, nonlinear resonance, and bifurcations [40,41]. Surprisingly, none of the previous studies, including damping and uniform periodic driving in nonlinear lattices, attempted to conduct such an analysis with DBs. In addition, these studies did not account for the effect of linear dispersion [33–39]. To the best our knowledge, highly spatially confined or compactlike DBs in a DNA lattice subjected to a uniform oscillating radiation field and damping, and with the presence of linear dispersion, have yet to be investigated. The present study focuses on DNA responses in a variety of DBs under such a physical context, including nonlinear resonance and spatiotemporal chaos.

It has been reported that impurities in driven and dissipative lattices can trap, reflect, or partially transmit propagating waves [42–44]. Although many authors have suggested that in the absence of dissipation and periodic driving force, an impurity in a DNA chain can trap and partially transmit the breather during its propagation [45–53], to the best of our knowledge taming the spatial and temporal dynamics of a driven and damped DNA lattice through an impurity has not yet been investigated.

To extend the previous work in this area, this paper investigates the existence of ILMs, orbital stability, and chaotic dynamics in a DNA model, including an impurity. Following the Introduction (Sec. I), the rest of the paper is structured as follows: In Sec. II, the JB model as well as its linear dispersion relation are derived. The ILMs are investigated by using the space-time separation of variables and the anticontinuum limit method. Also, the orbital stability is studied by means of Floquet's theory. In Sec. III, the nonlinear response of a single based pair as well as chaos taming using an impurity are analyzed. Section IV is devoted to a discussion of the obtained results as compared to what was observed in the literature. In Sec. V, the major achievements of the study are summarized, and a conclusion is provided.

II. THE DNA LATTICE MODEL

Let us consider the Joyeux-Buyukdagli (JB) model for DNA, whose Hamiltonian is given by [19,20]

$$H = \sum_n \frac{1}{2m}P_n^2 + D[1-\exp(-ay_n)]^2 + \frac{\Delta H}{C}[1-e^{-b(y_n-y_{n-1})^2}] + K_b(y_n-y_{n-1})^2, \quad (1)$$

where $P_n = m\dot{y}_n$ is the momentum, y_n represents the transverse stretching of the nucleotide pair at site n, and m denotes the mass of a nucleotide. The variables D and a are the depth and inverse width of the Morse potential. ΔH is a finite stacking energy, K_b is the harmonic elastic constant, and b is a spatial scale factor.

The dimensionless equation of motion corresponding to the Hamiltonian Eq. (1) is

$$\frac{d^2Y_n}{d\tau^2} + \frac{2K_b}{a^2D}(2Y_n - Y_{n+1} - Y_{n-1}) - 2(e^{-Y_n}-1)e^{-Y_n} + \frac{2b\Delta H}{a^2DC}[(Y_n - Y_{n-1})e^{-\frac{b}{a^2}(Y_n-Y_{n-1})^2}] - \frac{2b\Delta H}{a^2DC}[(Y_{n+1}-Y_n)e^{-\frac{b}{a^2}(Y_{n+1}-Y_n)^2}] = 0, \quad (2)$$

where $Y_n = ay_n$ and $\tau = t\sqrt{a^2D/m}$.

Breathers of small amplitudes qualitatively describe the DNA breathing modes and are thought to be the precursors of the bubbles that appear prior to the transcription processes [17,18]. To computationally study small-amplitude breathers, the original approach in [54] is used, and it is assumed that the oscillations of bases are large enough to be anharmonic, but still insufficient to break the bond since the plateau of Morse's potential is not reached. It is then presumed that the base nucleotides oscillate around the bottom of Morse's potential. On the one hand, the wave amplitude is considered big enough that the nonlinear effect that plays an essential role in the DNA molecules can still be incorporated [17,18]. On the other hand, it is still very small compared with the amplitude of a total separation of DNA nucleotide pairs. We can therefore expand the terms $\exp[-\frac{b}{a^2}(Y_{n\pm1}-Y_n)^2]$ and $\exp[-Y_n]$ in Eq. (2) up to second and third order, respectively [21–24]. Note that various regimes of motion (e.g., soliton, breather, and compacton) were investigated via likewise approximations, and they are supported by the original JB model [21–24].

To take into account the effect of viscosity of the medium as well as the influence of an external field, the JB original model is modified by incorporating $F_n(t) = A_n\cos(\omega t)$ and ν representing an external ac field and the effective damping of the system, respectively. From a physical viewpoint, external radiation effects on DNA are usually studied by means of artificial time-periodic external radiation that can be applied to the biomolecule from a laser source, an electronic device using a frequency up-conversion scheme, or an accelerating electron-based source [26]. Irradiations from biomedical imaging can be another controllable external source as well [25]. Therefore, the equation of motion can be written as

$$\ddot{Y}_n + \Gamma\dot{Y}_n - k_2(Y_{n+1} - 2Y_n + Y_{n-1}) + \omega_g^2\left(Y_n + \alpha Y_n^2 + \beta Y_n^3\right) - F_0\cos(\Omega\tau) + k_4[(Y_{n+1}-Y_n)^3 - (Y_n - Y_{n-1})^3] = 0. \quad (3)$$

The remaining coefficients of Eq. (3) are

$$\Gamma = \frac{\nu}{a}\sqrt{\frac{m}{D}}, \quad k_2 = \frac{2}{a^2D}\left(K_b + \frac{b\Delta H}{C}\right), \quad \omega_g^2 = 2, \quad F_0 = \frac{A_n}{aD}, \quad k_4 = \frac{2\Delta H b^2}{CDa^4}, \quad \alpha = -\frac{3}{2}, \quad \beta = \frac{7}{6}, \quad \Omega_g = \sqrt{\frac{a^2D}{m}}, \quad \Omega = \frac{\omega}{\Omega_g}. \quad (4)$$

By assuming $y_n(\tau) \propto \cos[qn - \Upsilon(q)\tau]$ in Eq. (3), retaining only linear terms, and discarding dissipation and driving, we can derive the following dispersion relation given by

TABLE I. Numerical values for the parameters [12,13].

Parameter	Value	Unit
m	300	amu
D	0.04	eV
a	4.45	Å^{-1}
b	0.10	Å^{-2}
ΔH	0.44	eV
K_b	10^{-5}	eV Å^{-2}
C	2	no unit

$\Upsilon(q) = \sqrt{\omega_g^2 + 4k_2 \sin^2(q/2)}$. It thus appears that the JB model is a pass band filter with a phonon band frequency between $\omega_{\min} = \omega_g$ and $\omega_{\max} = \sqrt{\omega_g^2 + 4k_2}$. In the first Brillouin zone ($q \in [0\,\pi]$) [55], using the values of parameters in Table I, the allowed frequency band is bound by the frequencies $\omega_{\min} = 1.4142$ and $\omega_{\max} = 1.4907$. In the following subsection, the existence of discrete breathers of Eq. (3) is investigated.

A. Discrete-breather generation by the time-space separability method

Let us assume that the nonlinear excitation solution of Eq. (3) is under the stationary form $Y_n(\tau) = \phi_n G(\tau)$ [34–39], with an arbitrary time-dependent amplitude $G(\tau)$ describing uniform oscillations of all the sites. After substitution of the previously mentioned ansatz $Y_n(\tau)$ into Eq. (3), the following equation is obtained:

$$\begin{aligned}&\phi_n \ddot{G}(\tau) + \Gamma\phi_n \dot{G}(\tau) - k_2(\phi_{n-1} - 2\phi_n + \phi_{n+1})G(\tau)\\&+ k_4 G^3(\tau)[(\phi_{n+1} - \phi_n)^3 - (\phi_n - \phi_{n-1})^3]\\&+ \omega_g^2\left[\phi_n G(\tau) + \alpha\phi_n^2 G^2(\tau) + \beta\phi_n^3 G^3(\tau)\right]\\&- F_0\cos(\Omega\tau) = 0.\end{aligned} \tag{5}$$

To understand the dynamics of different classes of solutions of Eq. (5), it is useful to start with a straightforward case restricted to the dynamics of a few coupled base pairs. This simple model gives a rather good approximation for the sites of a DB core, which are practically not affected by the presence of long-range interactions [35]. A simplification is further operated by taking into account only symmetric DBs centered at site $j = 0$ in the form $\phi_n = (0, \ldots, 0, \phi_{-2}, \phi_{-1}, \phi_0, \phi_1, \phi_2, 0, \ldots, 0)$, and then setting $\phi_{\pm(j+1)} = (-k_0)^{j+1}\phi_0$, with $j = 0, 1$, and k_0 a real parameter smaller than 1 ($|k_0| < 1$). This model approximation is a clear-cut scheme to design more complicated types of DBs with a tunable shape (varying ϕ_0 and k_0) [35]. After inserting this form of ϕ_n in Eq. (5), we obtain for the case $n = 0$ and 1 the following set of equations:

$$\begin{aligned}&\phi_0\ddot{G} + \Gamma\phi_0\dot{G} + \left[\omega_g^2 + 2k_2(1 + k_0)\right]\phi_0 G + \alpha\omega_g^2\phi_0^2 G^2\\&+ \left[\beta\omega_g^2 - 2k_4(1 + k_0)^3\right]\phi_0^3 G^3 - F_0\cos(\Omega\tau) = 0,\end{aligned} \tag{6}$$

$$\begin{aligned}&k_0\phi_0\ddot{G} + k_0\Gamma\phi_0\dot{G} + \left[k_0\omega_g^2 + k_2(1 + k_0)^2\right]\phi_0 G\\&- \alpha\omega_g^2 k_0^2\phi_0^2 G^2 + \left[\beta\omega_g^2 k_0^3 - k_4\left(1 + k_0^3\right)(1 + k_0)^3\right]\phi_0^3 G^3\\&+ F_0\cos(\Omega\tau) = 0.\end{aligned} \tag{7}$$

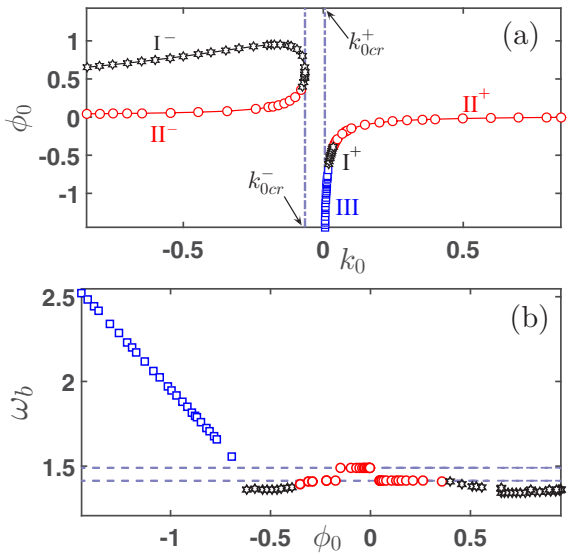

FIG. 1. (a) Real roots of Eq. (8) in the (k_0, ϕ_0) plane. In this figure, the dashed lines indicate the critical values of k_0 with $k^-_{0\mathrm{cr}} = -0.0653$ and $k^+_{0\mathrm{cr}} = 0.0056$. (b) DB frequency ω_b vs ϕ_0 for ILMs obtained in I$^-$, I$^+$, and III of the (k_0, ϕ_0) plane. The dashed lines indicate the location of the phonon band.

It should be noted that due to the symmetric term in Eq. (5), it is not possible to separate the space and temporal parts as in Refs. [34–39]. Inserting Eq. (6) into Eq. (7), one obtains the following nonlinear algebraic equation (see the details in the Appendix):

$$\begin{aligned}&k_4 G^3\phi_0^3 k_0^6 + 3k_4 G^3\phi_0^3 k_0^5 + k_4 G^3\phi_0^3 k_0^4 - \left[\beta\omega_g^2 G^3\phi_0^3\right.\\&\left.+ 4k_4 G^3\phi_0^3\right]k_0^3 + \left[\alpha\omega_g^2\phi_0^2 G^2 - 3k_4\phi_0^3 G^3 + k_2\phi_0 G\right]k_0^2\\&+ \left[k_4\phi_0^3 G^3 + \beta\omega_g^2\phi_0^3 G^3 + \alpha\omega_g^2\phi_0^2 G^2 - F_0\right]k_0 - k_2\phi_0 G\\&+ k_4\phi_0^3 G^3 - F_0 = 0.\end{aligned} \tag{8}$$

Without any loss of generality, it is assumed that $G(\tau = 0) = G = 1$. It is also assumed that the chain is initially nonexcited [$F_0(\tau = 0) = 0$]. The resolution of Eq. (8) makes it possible to know the couples (k_0, ϕ_0) for which the DBs exist. This resolution is made by means of the Newton-Raphson algorithm.

In Fig. 1(a), we report the roots of Eq. (8) in the range of parameters (k_0, ϕ_0). For the region $k_0 \leqslant k^-_{0\mathrm{cr}}$, there are two branches of the values of ϕ_0 that are solutions of Eq. (8), in particular the upper branch indexed by I$^-$ represented by a black hexagon, and the lower branch indexed by II$^-$ represented by a red circle. For $k_0 \in]k^-_{0\mathrm{cr}}, k^+_{0\mathrm{cr}}[$, Eq. (8) has no solution. When $k_0 \geqslant k^+_{0\mathrm{cr}}$, Fig. 1(a) exhibits one branch of solution that is further divided into three parts: III, I$^+$, and II$^+$, represented by blue squares, black hexagons, and red circles, respectively. It can be noticed that for low values of ϕ_0, the solutions are resonant with phonon modes (II$^-$ and II$^+$ branches) since their frequencies are in the allowed phonon band as depicted in Fig. 1(b) (zone in the red circle). I$^-$ and I$^+$ give localized mode solutions with dominant frequencies located in the lower forbidden band gap but closer to $\omega_{\min}$ [see the curve in the black hexagon in Fig. 1(b)], while part III gives localized mode solutions with frequencies located in

the upper forbidden band gap [see the curve in the blue square in Fig. 1(b)]. These DBs with fundamental frequencies in the forbidden band gaps (III and $I^{\pm}$) are prone to less radiation and might have the propensity to keep their shape for longer times [1,2]. It will therefore be interesting to carry out a stability analysis of the ILM belonging to the branches I^{-}, I^{+}, and III in order to see if such excitation is suitable for the energy localization and transfer in the DNA in the context of periodic driving and dissipation.

In physical applications, it is expedient to consider the solutions that are stable against small perturbations. Thus once a given DB solution $\hat{Y}_n(\tau)$ is obtained, we add a small perturbation to it $[Y_n(\tau) = \hat{Y}_n(\tau) + \epsilon_n(\tau)]$ and linearize the equation of motion (3) with respect to $\epsilon_n(\tau)$:

$$\begin{aligned}\ddot{\epsilon}_n - k_2(\epsilon_{n+1} - 2\epsilon_n + \epsilon_{n-1}) + \omega_g^2\left(1 + 2\alpha\hat{Y}_n + 3\beta\hat{Y}_n^2\right)\epsilon_n \\ - 3k_4[(\hat{Y}_{n+1} - \hat{Y}_n)^2(\epsilon_{n+1} - \epsilon_n) \\ + (\hat{Y}_{n-1} - \hat{Y}_n)^2(\epsilon_{n-1} - \epsilon_n)] = 0. \end{aligned} \tag{9}$$

Let us note that to obtain Eq. (9), the coefficient of dissipation is canceled since we seek nondissipative initial solutions. To identify the orbital stability of these solutions, Floquet's analysis can be performed. Floquet's method is the commonly accepted method for DB stability analysis. A solution $\hat{Y}_n(\tau)$ is considered stable when, for any initial conditions, the linear perturbation $\epsilon_n(\tau)$ does not grow exponentially with time. When $\hat{Y}_n(\tau)$ is time-periodic with period T_b, then Eq. (9) defines a linear symplectic map between the initial perturbation at $\tau = 0$ and the perturbation at time $\tau = T_b$, expressed by a matrix $\mathcal{M} = \mathcal{M}(\hat{Y}_n)$, known as the monodromy matrix:

$$\begin{bmatrix}\epsilon_n(T_b) \\ \dot{\epsilon}_n(T_b)\end{bmatrix} = \mathcal{M}\begin{bmatrix}\epsilon_n(0) \\ \dot{\epsilon}_n(0)\end{bmatrix}. \tag{10}$$

The complex eigenvalues λ and eigenvectors of the $2N \times 2N$ monodromy matrix $\mathcal{M}$ provide information about the stability of the DB. If all eigenvalue moduli $|\lambda|$ are less than (or equal to) 1, then the DB is linearly (or marginally) stable. Otherwise perturbations persisting and growing with time (typically exponentially) correspond to a linearly unstable DB.

The study of the orbital stability of ILMs derived from Fig. 1(a) is performed over an interval of five DB periods ($\tau = 5T_b$ with $T_b = 2\pi/\omega_b$). The results are represented in Fig. 2, which shows three types of solutions taken on branches I^{-}, I^{+}, and III, with the corresponding Floquet multiplier on a unit circle, as well as the corresponding power spectrum. We can also observe that some solutions in branches I^{-} and I^{+}, which possess nondominant frequencies inside the phonon band, are linearly unstable since some eigenvalues of their monodromy matrices leave the unit circle outward [see Figs. 2(b) and 2(e)]. However, the intrinsic localized modes of branch III of Fig. 1(a) are marginally stable [see Fig. 2(h)].

B. Discrete breather generation by continuation to the anticontinuous limit: Effects of dissipation and external driving

From the previous analysis, the DBs were estimated without dissipation and external force for specific values of system parameters. Thus in what follows, taking into account those

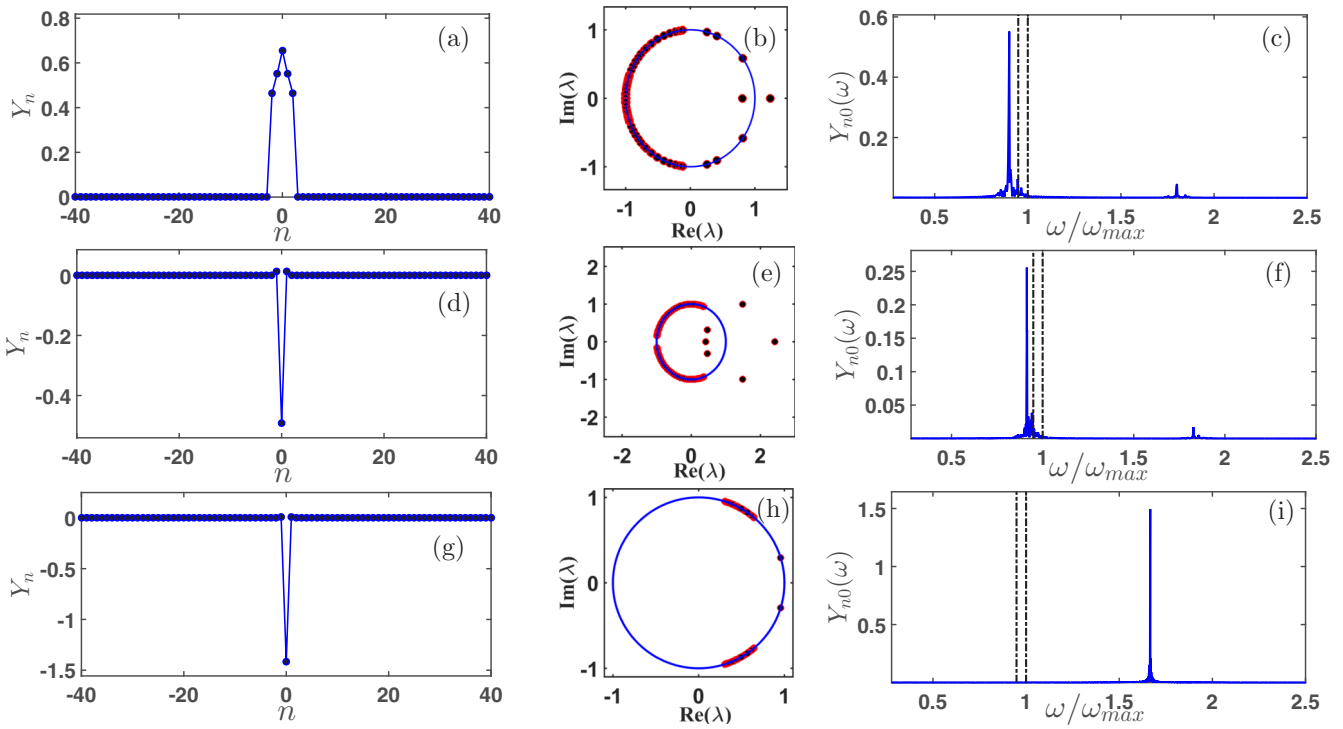

FIG. 2. Discrete breather profiles taken in branches I^{-}, I^{+}, and III for (a) $k_0 = -0.8426$, $\phi_0 = 0.6546$; (d) $k_0 = 0.0267$, $\phi_0 = -0.4915$; and (g) $k_0 = 0.0061$, $\phi_0 = -1.415$, respectively, and corresponding Floquet multiplier spectra [middle column (b), (e), and (h)]. The right column [(c), (f), and (i)] depicts power spectra of each ILM (the dashed lines indicate the location of the phonon band). For all these panels, $F_0 = 0$ and $\Gamma = 0$.

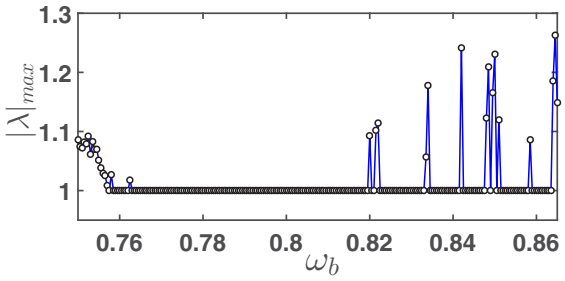

FIG. 3. Evolution with respect to the DB frequency ω_b of the maximum modulus of the Floquet multiplier with $F_0 = 0$, $\Gamma = 0$.

effects, the ILM with arbitrary frequency $f_b = \omega_b/2\pi$ in the forbidden band gap is estimated regardless of the restrictions imposed by the branches of existence calculated previously. The DBs are spatially localized time-periodic solutions to the nonlinear system of equations of motion in terms of $Y_n(\tau)$. They are calculated as fixed points of the map,

$$\mathcal{P} : \begin{bmatrix} Y_n(0) \\ \dot{Y}_n(0) \end{bmatrix} \longmapsto \begin{bmatrix} Y_n(T_b) \\ \dot{Y}_n(T_b) \end{bmatrix}, \tag{11}$$

where $T_b = 1/f_b$ is the temporal period of the DB. The estimate of the periodic DB solution of Eq. (3) is made by using Newton's method combined with the anticontinuous limit described in [56]. This procedure is useful for obtaining solutions with relatively high accuracy.

Figure 3 shows the absolute value of Floquet's multipliers λ for a one-site DB versus the driving frequency ω_b. It can be seen that there are very few values of ω_b for which the discrete breathers centered on one site are unstable.

Figure 4 illustrates two types of solutions whose DB frequencies are worth, respectively, $\omega_b = 0.8$ [Fig. 4(a) for $F_0 = 0$, $\Gamma = 0$ and Fig. 4(c) for $F_0 = 0.75$, $\Gamma = 0$] and $\omega_b = 0.75$ [Fig. 4(b) for $F_0 = 0$, $\Gamma = 0$ and Fig. 4(d) for $F_0 = 0.75$, $\Gamma = 0$]. These solutions, obtained by the anticontinuous limit, have their Floquet multipliers projected on the unit circle (inset curve). The corresponding power spectrum of these solutions (not shown here) reveals that these discrete breathers have their frequency above the upper cutoff frequency of the forbidden band of the phonon's mode. The linear instability of the solution obtained for $\omega_b = 0.75$ in the absence of viscosity and periodic force is certainly due to the interaction of the weak frequencies of its corresponding power spectrum with the phonon's mode. Curves (c) and (d) of Fig. 4 illustrate the intrinsic localized modes in the presence of the driving force only, and it arises that these solutions are linearly unstable for the value $F_0 = 0.75$.

For the choice of frequency $\omega_b = 0.8$, we also generated DBs by taking into account simultaneously the viscosity of the medium and the external force. These discrete breathers take form for small values of Γ and F_0 as predicted in [57]. Figure 5(a) represents this discrete breather and its corresponding Floquet spectrum arising from its linear stability. After building this discrete breather in the presence of dissipation and external driving, the robustness of this solution is subsequently checked. Figures 5(b) and 5(c) depict the absolute value and argument (inset curves) of the eigenvalues of the DB with $\omega_b = 0.8$, $F_0 = 0.06$. An instability is observed for a critical viscosity $\nu_{cr} = 0.087$ ps^{-1} [Fig. 5(b)], while in Fig. 5(c) there is a very close domain where the constructed discrete breather is marginally stable. Let us note that for increasingly significant values of F_0, the generated discrete breathers become increasingly unstable.

In the following section, we will analyze the influence of the impurity on DNA dynamics subjected to periodic excitation.

III. EFFECT OF THE IMPURITY ON DNA DYNAMICS

It is well known that the DNA molecule can be subjected to genetic changes during the transmission of hereditary features

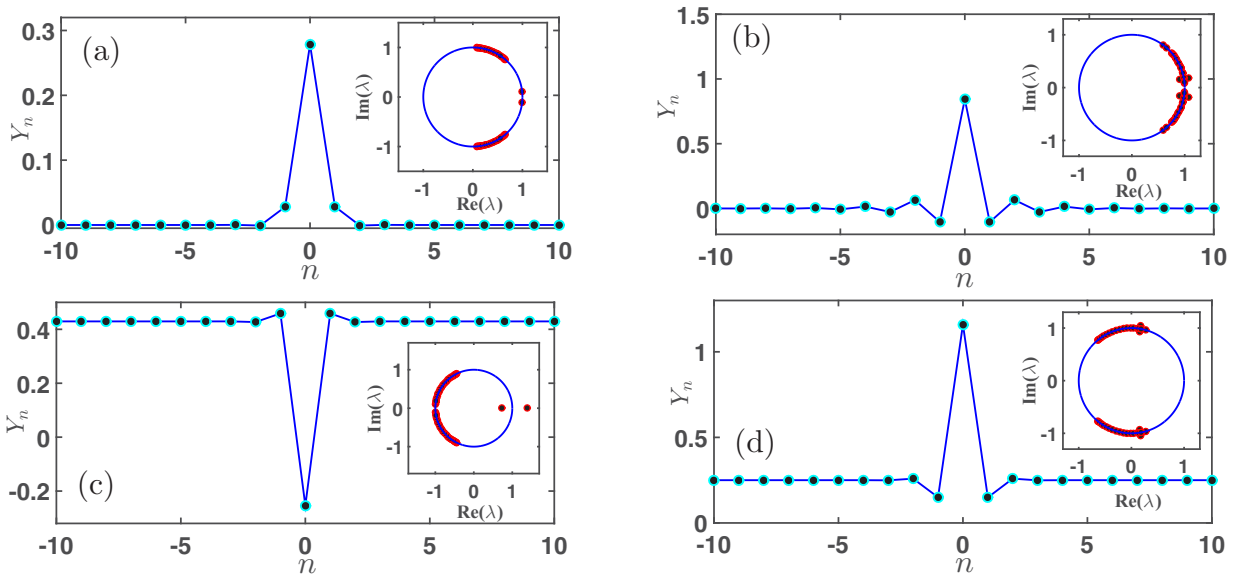

FIG. 4. Discrete breather profiles for $\omega_b = 0.8$ [(a) $F_0 = 0$, $\Gamma = 0$; (c) $F_0 = 0.75$, $\Gamma = 0$] and for $\omega_b = 0.75$ [(b) $F_0 = 0$, $\Gamma = 0$; (d) $F_0 = 0.75$, $\Gamma = 0$]. The inset shows the corresponding Floquet multiplier spectra of these DBs.

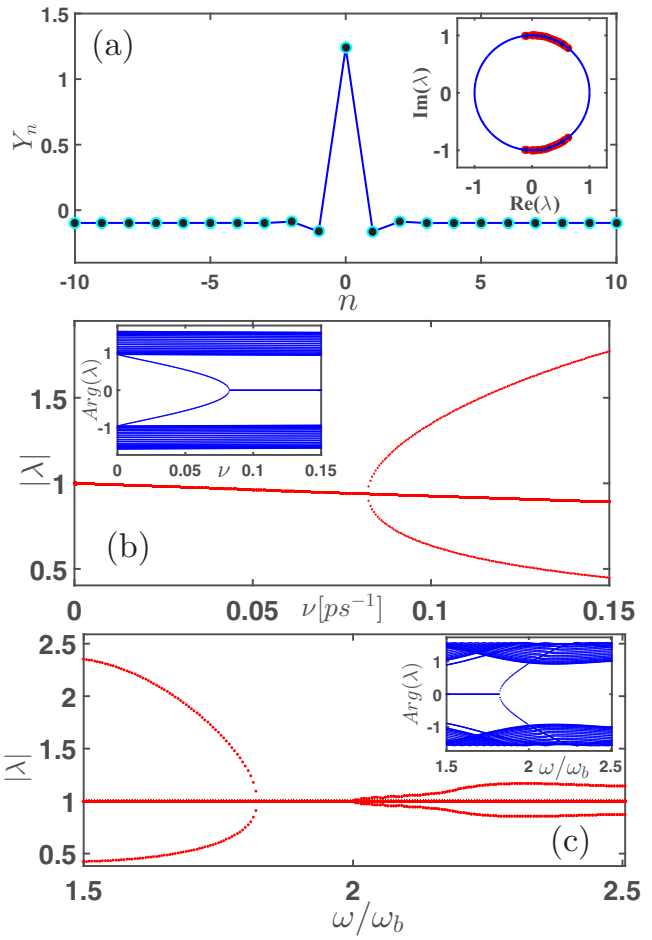

FIG. 5. (a) Discrete breather profiles under periodic driving and viscosity and the corresponding Floquet multiplier spectra for $\omega_b = 0.8$, $\Omega = 2\omega_b$, $F_0 = 0.06$, and $\Gamma \approx 1.95 \times 10^{-4}$. Panels (b) and (c) display the absolute value and argument (inset) of the eigenvalues of the continued discrete breather.

from one generation to another. These changes can have dramatic consequences on the descendents of a specie. The genetic changes can be centered in a precise site, or extended on a portion of the DNA. In the present section, we are interested in the change that is centered on a site. Taking into account the fact that in the DNA molecule the hydrogen bonds between adenine and thymine are about 2, whereas between guanine and cytosine they are about 3, a change of this configuration can lead to another sequence that can be view as an impurity. Thus, the impurity throughout this section will be defined by the coefficients of the Morse potential, symbolizing the interaction between the pairs of bases.

It is of primary importance to start with the study of only one base pair subjected to the action of a periodic force and the viscosity. This will enable us to gain insight into the characteristics of the amplitude response of the system according to the frequency of the external force. It allows us to better probe and spot which features of the single cell are crucial for the emergence of the collective phenomenon of localization in the lattice. Thus, the dynamics of an uncoupled basic pair ($k_2 = k_4 = 0$) is given by the equation

$$\ddot{Y}_n(\tau) + \Gamma\dot{Y}_n(\tau) + \sum_{j=1}^{3}\alpha_j Y_n^j(\tau) = F_0\cos(\Omega\tau),$$
$$\alpha_1 = \omega_g^2, \quad \alpha_2 = \alpha\omega_g^2, \quad \alpha_3 = \beta\omega_g^2. \tag{12}$$

Due to the nonlinearity of Eq. (12), it is very difficult to obtain the exact solution. However, techniques were developed in the literature to approach an analytical solution. One of these is the harmonic balance method, which approximates periodic solutions of nonlinear differential equations by finite sums of trigonometric functions [40]. To do so, it is assumed that the periodic-like response of Eq. (12) can be written as

$$Y_n(\tau) = B_0 + A_1\cos(\Omega\tau) + A_2\sin(\Omega\tau), \tag{13}$$

where B_0, A_1, and A_2 are the coefficients to be determined. Substituting Eq. (13) into Eq. (12) and equating the coefficients of the constant term and the first-harmonic components, we obtain

$$\begin{aligned}
-\Gamma\Omega A_1 + \left[\left(3B_0^2 + \tfrac{3}{4}A^2\right)\alpha_3 + 2\alpha_2 B_0 + \alpha_1 - \Omega^2\right]A_2 &= 0,\\
\left[\left(3B_0^2 + \tfrac{3}{4}A^2\right)\alpha_3 + 2\alpha_2 B_0 + \alpha_1 - \Omega^2\right]A_1 + \Gamma\Omega A_2 &= F_0,\\
\left(B_0^2 + \tfrac{3}{2}A^2\right)\alpha_3 B_0 + \left(B_0^2 + \tfrac{1}{2}A^2\right)\alpha_2 + \alpha_1 B_0 &= 0,
\end{aligned} \tag{14}$$

where $A^2 = A_1^2 + A_2^2$. The decoupling of B_0 from A_1 and A_2 in Eqs. (14) yields after some arrangements the following nonlinear algebraic equation:

$$\sum_{j=0}^{9} e_j B_0^j = 0, \tag{15}$$

where the coefficients e_j are

$$e_0 = 2F_0^2\alpha_3^2,$$
$$e_1 = 4\alpha_1\alpha_2\left[(\Omega^2 - \alpha_1)^2 + \Omega^2\Gamma^2 + \frac{9F_0^2\alpha_3}{2\alpha_1}\right],$$
$$e_2 = 4\alpha_2\left(\alpha_2^2 + 6\alpha_1\alpha_3\right)\Omega^4 + 4\alpha_2\left[(\Gamma^2 - 6\alpha_1)\alpha_2^2 + 3\alpha_1\alpha_3(\Gamma^2 - 3\alpha_1)\right]\Omega^2 + 4\alpha_2\left[5\alpha_1^2\alpha_2^2 + 3\alpha_1^3\alpha_3 + \frac{27}{2}F_0^2\alpha_3^2\right],$$
$$e_3 = 4\alpha_3\left(9\alpha_1\alpha_3 + 7\alpha_2^2\right)\Omega^4 + 4\alpha_3\left[9\alpha_1\alpha_3(\Gamma^2 - \alpha_1) + (7\Gamma^2 - 38\alpha_1)\alpha_2 - 4\frac{\alpha_2^4}{\alpha_3}\right]\Omega^2 + 32\alpha_1\alpha_2^4 + 54\alpha_3^3F_0^2 + 9\alpha_3^2\alpha_1^3$$
$$+ 100\alpha_1^2\alpha_2^2\alpha_3,$$

$$
\begin{aligned}
e_4 &= 60\alpha_2\alpha_3^2\Omega^4 + 4\alpha_2\alpha_3\left[3\alpha_3(5\Gamma^2 - 26\alpha_1) - 31\alpha_2^2\right]\Omega^2 + 16\alpha_2^5 + 171\alpha_1^2\alpha_3^2\alpha_2 + 220\alpha_1\alpha_3\alpha_2^3,\\
e_5 &= 36\alpha_3^3\Omega^4 + 12\alpha_3^2\left[3\alpha_3(\Gamma^2 - 6\alpha_1) - 29\alpha_2^2\right]\Omega^2 + 99\alpha_1^2\alpha_3^3 + 136\alpha_3\alpha_2^4 + 579\alpha_1\alpha_2^2\alpha_3^2,\\
e_6 &= 5\alpha_2\alpha_3^2\left[-84\alpha_3\Omega^2 + 93\alpha_2^2 + 138\alpha_1\alpha_3\right],\\
e_7 &= -180\alpha_3^4\Omega^2 + 15\alpha_3^3\left(21\alpha_1\alpha_3 + 53\alpha_2^2\right),\\
e_8 &= 675\alpha_2\alpha_3^4,\\
e_9 &= 225\alpha_3^5.
\end{aligned}
\tag{16}
$$

For any value of B_0 obtained from Eqs. (15), A_1 and A_2 can be determined using Eqs. (14). Then, the amplitude-frequency response relationship can be calculated by

$$\mathscr{A} = |B_0| + \sqrt{A_1^2 + A_2^2}. \tag{17}$$

Using the Newton-Raphson algorithm, one finds B_0 when the frequency Ω varies.

Figure 6 shows the extreme amplitude-frequency $[\max(Y_n) = \mathscr{A}]$ and the response of the single base pair, obtained analytically and numerically by integrating Eq. (12) with the standard fourth-order Runge-Kutta algorithm. This figure shows the value of the frequency of the external force to be avoided because it is responsible for the occurrence of the resonance as well as jump phenomena. Thus, in the rest of the paper it is considered that $\Omega = 1.2$. Taking into account the fact that F_0 has an enormous influence on the amplitude response of the system, it is primordial to know the response of the unit cell for varying values of the amplitude F_0. Figure 7 represents the bifurcation diagram of a single base pair under periodic excitation. One observes in this figure that there are values of F_0 for which the dynamics of a unit cell exhibits chaotic, quasiperiodic, or periodic behavior.

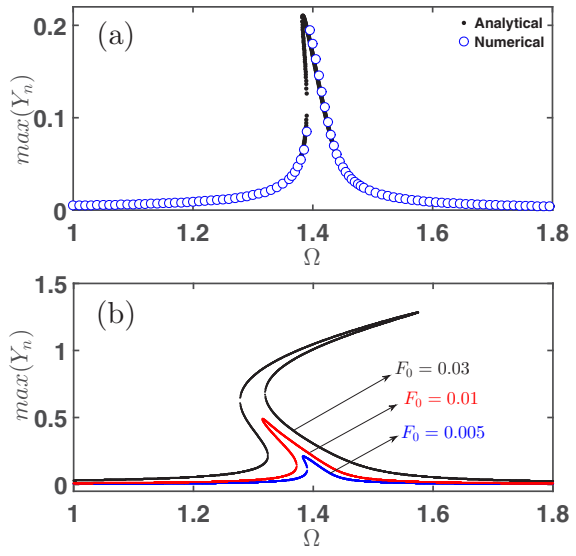

FIG. 6. (a) Extreme amplitude-frequency responses of a single base pair $[\max(Y_n) = \mathscr{A}]$, obtained analytically (shown by a dot) and numerically (shown by a circle) from the integration of Eq. (12) with $F_0 = 0.005$. (b) Extreme amplitude-frequency response of a single base for different values of drive intensity and with $\Gamma = 1.952 \times 10^{-2}$ [the numerical curves with the same method of (a) were found concordant with this analytical result of (b). It was not shown here for the sake of clarity and to avoid an overload of the graphs].

Knowing the chaotic behavior of the unit cell under periodic excitation, it is of primary importance to explore the dynamics of the coupled system in the presence of an impurity. Let us analyze the influence of a specific impurity in the DNA by taking into account the presence of a periodic force and viscosity. For that purpose, the new coefficients of the Morse potential, including the impurity localized at a site n_0, are $a_n' = [(\mu - 1)\delta_{nn_0} + 1]a$ and $D_n' = [(\mu - 1)\delta_{nn_0} + 1]D$, with $0.399 \leqslant \mu \leqslant 1.5$ and δ_{nn_0} denoting the Kronecker symbol.

For all the upcoming numerical simulations, the driving amplitude and the frequency values are chosen as $F_0 = 8$ and $\Omega = 1.2$. Moreover, free boundary conditions are assumed. For these previous specific values, a single DNA base pair exhibits a strange attractor, a large number and dense set of orbits in the phase space, and a strictly positive Lyapunov exponent (results not shown in the paper). To detect the chaotic behavior of a whole DNA molecule subjected to the influence of the impurity, it is more convenient to measure the average speed of the pairs of bases given by

$$\sigma(jT) = \frac{1}{N}\sum_{n=1}^{n=N}\dot{Y}_n(jT), \tag{18}$$

at times that are integer multiples of the forcing period $T = 2\pi/\Omega$. This measure is computed at each period, and it is plotted as a function of jT, i.e., at each subsequent period.

Figure 8 shows the average base-pair velocity $\sigma(\tau)$ at $\tau = 30T, 31T, \ldots, 40T$ as a function of μ. This global bifurcation of the whole lattice according to the value of the impurity is

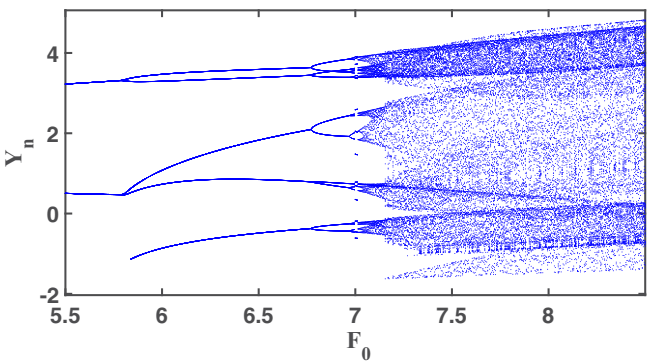

FIG. 7. Bifurcation diagram of a single base pair as a function of F_0 with $\Omega = 1.2$.

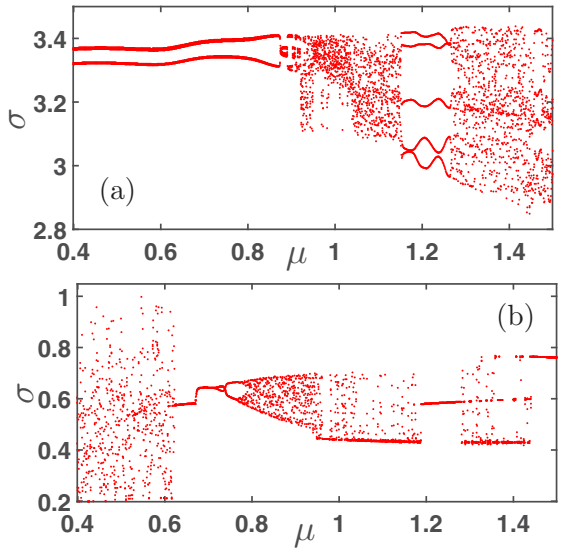

FIG. 8. Chaotic and regular dynamics as a function of the degree of impurity. The average velocity at $\tau = 30T, 31T, \ldots, 40T$ is shown for each value of impurity parameter μ. Top panel: for $n \neq n_0$, $V_M = 0.8D(e^{-0.8ay_n} - 1)^2$; bottom panel: for $n \neq n_0$, $V_M = 1.2D(e^{-1.2ay_n} - 1)^2$.

depicted. It can be clearly seen that when the parameter μ of the impurity matches that of the other sites of the lattice, all the base pairs vibrate collectively with a high number of local minima. This means that the coupling between DNA base pairs does not inhibit the chaotic dynamics of isolated elements indicated before. In comparison with the bifurcation curve given in Fig. 8, we observe that when the Morse potential is not very deep, the behavior of the chains subjected to an impurity exhibits two quasiperiodic zones obtained for $0.399 \leqslant \mu \leqslant 0.921$ and $1.152 \leqslant \mu \leqslant 1.272$ [see Fig. 8(a)].

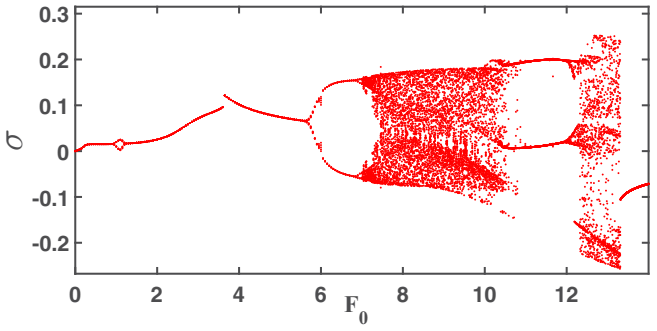

FIG. 10. Chaotic and regular dynamics of a single excited DNA base pair at site n_0 vs the amplitude of the exiting force F_0. $\Omega = 1.2$, $D = 0.04$ eV, and $a = 4.45$ Å^{-1}.

The chain becomes chaotic for all other values of μ out of these intervals. Figure 8(b) obtained for a deeper Morse potential exhibits three zones where the chain has a chaotic behavior (for $0.399 \leqslant \mu \leqslant 0.623$, $0.783 \leqslant \mu \leqslant 1.188$, and $1.28 \leqslant \mu \leqslant 1.44$) and quasiperiodic dynamics elsewhere. It is observed that a nonintrinsic localized mode can remain quasiperiodic with time (Fig. 9, top left and bottom left), or it can still be present without inhibition of the collective chaotic vibration of the lattice (Fig. 9, top right and bottom right). Surprisingly, the same phenomena occur when only a single site of the lattice is excited (Fig. 10). For a homogeneous DNA chain, periodic driving applied to one site can induce either chaotic or regular collective motion.

IV. DISCUSSION

Most of the analytical studies devoted to the understanding of driven and damped nonlinear lattices in which DBs are explicitly constructed by an exact separation of their time and space dependence possessed models with either purely

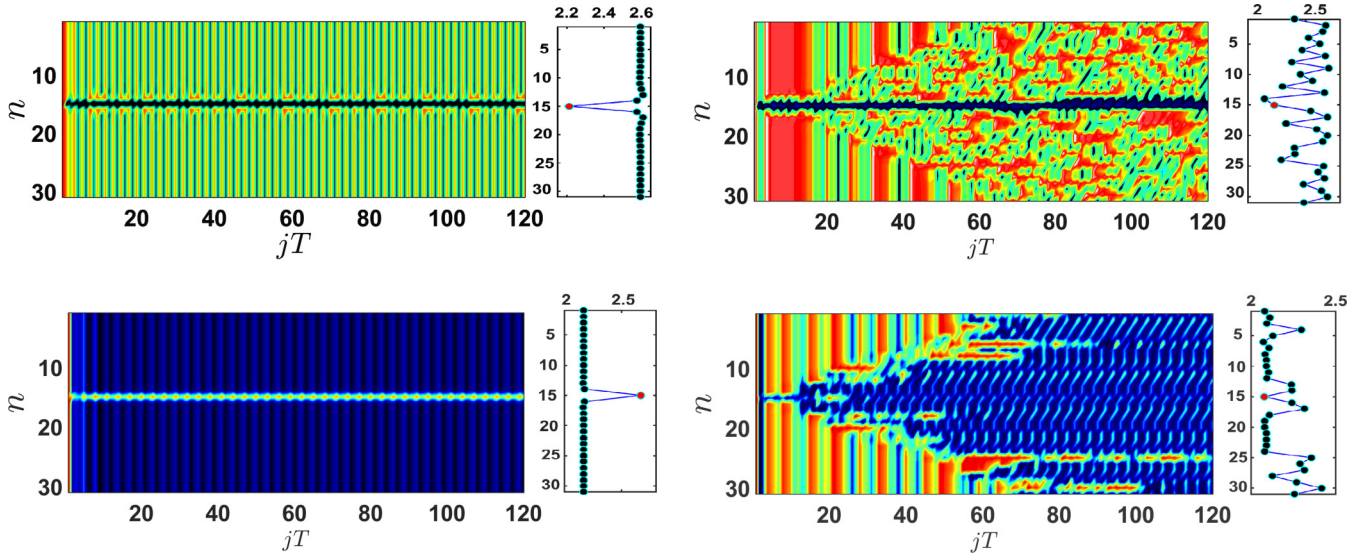

FIG. 9. Spatiotemporal position patterns for chaotic and regular dynamics in an array of $N = 31$ coupled DNA base pairs. Top left panel: for $n \neq n_0$, $(a'_n, D'_n) = 0.8(a, D)$, at $n = n_0$ $(a'_n, D'_n) = 1.215(a, D)$; top right panel: for $n \neq n_0$, $(a'_n, D'_n) = (a, D)$, at $n = n_0$ $(a'_n, D'_n) = 1.215(a, D)$. Bottom left panel: for $n \neq n_0$, $(a'_n, D'_n) = 1.2(a, D)$, at $n = n_0$ $(a'_n, D'_n) = 0.688(a, D)$; bottom right panel: for $n \neq n_0$, $(a'_n, D'_n) = 1.378(a, D)$, at $n = n_0$ $(a'_n, D'_n) = 1.2(a, D)$. These coefficient values of the Morse potential are taken from Figs. 8(a) and 8(b), respectively.

anharmonic short-range interaction potentials, nonlinear on-site potential, or nonlinear dispersion [33–39]. By using a simplified DB core structure as in Ref. [36], the present study provided rich families and several branches of ILM solutions in which there are branches of orbital stability and instability as well as the mixing of them. We showed that the dominant frequency of the DBs falls mostly outside the phonon band, which is naturally expected for nonlinear ILMs [3,57]. Note that this method of separation of variables was mostly applied in nonlinear lattices, where there is no linear dispersion and thus no phonon band [34,36]. This is not the case in the present study. In the current research work, the core model is reduced into an algebraic equation in which the existence of discrete ILMs is demonstrated. Note that Ndjoko *et al.* [23] and Gninzanlong *et al.* [24], respectively, obtained highly spatially confined solitons from continuous and discrete versions of the JB model without external driving and dissipation.

It was reported that impurities in driven and damped nonlinear electrical lattices can be used for movement control of ILMs [10,14], as well as for phase synchronization of vibrations of coupled pendulums [58,59]. These imperfections in the lattice modify the nonlinear frequency response of the system [60–62]. As compared to the previously mentioned studies [10,14,58–60,62], here it is demonstrated that a single defect in the local potential energy of the nonlinear chain can produce a nonintrinsic localized mode as well as synchronized spatiotemporal patterns when the entire set of oscillators and the impurity exhibit chaotic behavior. Moreover, it is shown that the periodic excitation applied at a specific single site can create regular spatial and temporal patterns in the whole lattice even if all sites are in a chaotic environment. This implies that the impurity and driving can be used as control parameters on the dynamics of the nonlinear chain. The nonlinear frequency response of a homogeneous, driven, and damped nonlinear lattice was analyzed [63–66]. However, the discrete waves constructed in these studies were not exponentially localized, possibly due to the resonance between phonon modes and the ILM [67].

The localized mode formation in driven and damped DNA was studied mostly by observing bifurcations and numerical simulations in the Dauxois-Peyrard-Bishop model [29–32]. Stacking interactions between neighbor bases along the DNA axis stabilize the secondary DNA structure. They hold one base over the next one and form a stack of bases [17]. This stacking interaction, however, does not incorporate any characteristic energy associated with it [18]. Inspired by the anharmonic model suggested by DPB, Joyeux and Buyukdagli (JB) proposed a new model based on site-specific enthalpy that is closer to the statistical models [19,20]. This study accounted for the damping and driving as in Refs. [29–32], but it investigated the generation of staggered or unstaggered discrete ILMs and their stability based on the JB model. The nonlinear response of the DNA as a function of driver amplitude and frequency was also analyzed. In the absence of dissipation and periodic driving force, the impurity in the DNA chain can trap, partially transmit, or reflect the breather during its propagation [45–53]. Here it is demonstrated that a base pair with different potential energy of interaction (impurity) can suppress or induce the spatial and temporal chaotic dynamics.

The model used here has been proposed by Joyeux and Buyukdagli to explain homogeneous and inhomogeneous DNA denaturation and the finite stacking enthalpy energy of base pairs [19,20]. This underscores the fact that our results can be useful to explore some properties of DNA chains. To illustrate this, if a DNA molecule exposed to external radiation and viscous damping can corner the energy at the inhomogeneity, these factors can therefore foster the occurrence of a transcription bubble [17]. These trapped ILMs may therefore operate as energy pools and can reassign this encapsulated energy to a localized and propagating transcription bubble. It is reported that periodic excitation on a DNA lattice can induce stable or unstable base-pair vibration or accelerate the separation of the double helix into single helices [29–32]. However, in the presence of such external forcing and damping, as expected for most nonlinear systems, the DNA lattice can undergo a transition to chaos. Nevertheless, the results obtained in the present study suggest that a suitable balance between the effect of these external factors and inhomogeneity can prevent and control the chaotic spatiotemporal dynamics.

V. CONCLUSION

In this paper, the formation of ILMs, their stability, and their chaotic dynamics are studied in damped and periodically driven DNA. The effect of inhomogeneity on the spatiotemporal dynamics is also investigated. The regions of existence and stability of one-peak unstaggered ILMs were characterized. These coherent localized modes of different kinds were also classified on the basis of stability properties and their corresponding Floquet spectra. It is demonstrated that a chain of chaotic DNA base pairs can be frequency-locked into a spatiotemporal pattern by incorporating a proper impurity at a site in the lattice. In most cases, a single impurity can tame chaos. It is found that a single nonchaotic defect with an appropriate Morse potential depth can control and organize the dynamics of the lattice. Increasing the potential depth increases the depth domain of the impurity base pair for which the organization can be observed. It is shown that when the periodic excitation is only applied at a specific single site, it can create regular spatial and temporal patterns in the whole lattice even when all the sites are in a chaotic regime.

ACKNOWLEDGMENTS

We thanks the Electronic Journal Delivery Service of the International Centre of Theoretical Physics (ICTP) for providing valuable references used in this study. The help of Patrick Guemkam Ghomsi of the University of Buea at the early stage of this work is gratefully acknowledged. We thank the reviewers for their comments, which improved this paper significantly.

APPENDIX: DERIVATION OF EQ. (8)

In this Appendix, we explain the procedure that allowed us to obtain the algebraic equation (8). Let us rewrite Eqs. (6) and (7) as the following Eqs. (A1) and (A2),

respectively:

$$\phi_0\ddot{G} + \Gamma\phi_0\dot{G} = F_0\cos(\Omega\tau) - \left[\omega_g^2 + 2k_2(1+k_0)\right]\phi_0 G - \alpha\omega_g^2\phi_0^2G^2 - \left[\beta\omega_g^2 - 2k_4(1+k_0)^3\right]\phi_0^3G^3, \tag{A1}$$

$$k_0\phi_0\ddot{G} + k_0\Gamma\phi_0\dot{G} = -F_0\cos(\Omega\tau) + \alpha\omega_g^2k_0^2\phi_0^2G^2 - \left[\beta\omega_g^2k_0^3 - k_4\left(1+k_0^3\right)(1+k_0)^3\right]\phi_0^3G^3 - \left[k_0\omega_g^2 + k_2(1+k_0)^2\right]\phi_0 G. \tag{A2}$$

The multiplication of Eq. (A1) by k_0 leads to

$$k_0\phi_0\ddot{G} + k_0\Gamma\phi_0\dot{G} = k_0F_0\cos(\Omega\tau) - k_0\alpha\omega_g^2\phi_0^2G^2 - k_0\left[\beta\omega_g^2 - 2k_4(1+k_0)^3\right]\phi_0^3G^3 - k_0\left[\omega_g^2 + 2k_2(1+k_0)\right]\phi_0 G. \tag{A3}$$

It can be observed that the left-hand side of Eq. (A3) is identical to the left-hand side of Eq. (A2). With a substitution of the term $(k_0\phi_0\ddot{G} + k_0\Gamma\phi_0\dot{G})$ obtained from Eq. (A3) by its expression into Eq. (A2) and by collecting the terms in k_0, we obtain

$$\begin{aligned} &k_4G^3\phi_0^3k_0^6 + 3k_4G^3\phi_0^3k_0^5 + k_4G^3\phi_0^3k_0^4 - \left[\beta\omega_g^2G^3\phi_0^3 + 4k_4G^3\phi_0^3\right]k_0^3 + \left[\alpha\omega_g^2\phi_0^2G^2 - 3k_4\phi_0^3G^3 + k_2\phi_0 G\right]k_0^2 \\ &+ \left[k_4\phi_0^3G^3 + \beta\omega_g^2\phi_0^3G^3 + \alpha\omega_g^2\phi_0^2G^2 - F_0\cos(\Omega\tau)\right]k_0 - k_2\phi_0 G + k_4\phi_0^3G^3 - F_0\cos(\Omega\tau) = 0. \end{aligned} \tag{A4}$$

Equation (A4) is reduced to Eq. (8) by setting $\tau = 0$.

[1] S. Flach and A. V. Gorbach, Discrete breathers—Advances in theory and applications, Phys. Rep. **467**, 1 (2008).

[2] S. Flach and C. R. Willis, Discrete breathers, Phys. Rep. **295**, 181 (1998).

[3] D. K. Campbell, S. Flach, and Y. S. Kivshar, Localizing energy through nonlinearity and discreteness, Phys. Today **57**(1), 43 (2004).

[4] D. Zueco, P. J. Martinez, L. M. Floría, and F. Falo, Mode-locking of mobile discrete breathers, Phys. Rev. E **71**, 036613 (2005).

[5] P. J. Martinez, M. Meister, L. M. Floria, and F. Falo, Dissipative discrete breathers: Periodic, quasiperiodic, chaotic, and mobile, Chaos Interdisc. J. Nonlin. Sci. **13**, 610 (2003).

[6] Y. Xu, T. J. Alexander, H. Sidhu, and P. G. Kevrekidis, Instability dynamics and breather formation in a horizontally shaken pendulum chain, Phys. Rev. E **90**, 042921 (2014).

[7] F. Palmero, J. Han, L. Q. English, T. J. Alexander, and P. G. Kevrekidis, Multifrequency and edge breathers in the discrete sine-Gordon system via subharmonic driving: Theory, computation and experiment, Phys. Lett. A **380**, 402 (2016).

[8] J. Cuevas, L. Q. English, P. G. Kevrekidis, and M. Anderson, Discrete Breathers in a Forced-Damped Array of Coupled Pendula: Modeling, Computation, and Experiment, Phys. Rev. Lett. **102**, 224101 (2009).

[9] L. Q. English, F. Palmero, J. F. Stormes, J. Cuevas, R. Carretero-González, and P. G. Kevrekidis, Nonlinear localized modes in two-dimensional electrical lattices, Phys. Rev. E **88**, 022912 (2013).

[10] L. Q. English, F. Palmero, A. J. Sievers, P. G. Kevrekidis, and D. H. Barnak, Traveling and stationary intrinsic localized modes and their spatial control in electrical lattices, Phys. Rev. E **81**, 046605 (2010).

[11] L. Q. English, R. B. Thakur, and R. Stearrett, Patterns of traveling intrinsic localized modes in a driven electrical lattice, Phys. Rev. E **77**, 066601 (2008).

[12] L. Q. English, F. Palmero, P. Candiani, J. Cuevas, R. Carretero-Gonzalez, P. G. Kevrekidis, and A. J. Sievers, Generation of Localized Modes in an Electrical Lattice Using Subharmonic Driving, Phys. Rev. Lett. **108**, 084101 (2012).

[13] M. Sato, T. Mukaide, T. Nakaguchi, and A. J. Sievers, Inductive intrinsic localized modes in a one-dimensional nonlinear electric transmission line, Phys. Rev. E **94**, 012223 (2016).

[14] F. Palmero, L. Q. English, J. Cuevas, R. Carretero-Gonzalez, and P. G. Kevrekidis, Discrete breathers in a nonlinear electric line: Modeling, computation, and experiment, Phys. Rev. E **84**, 026605 (2011).

[15] M. Kimura and T. Hikihara, A study on intrinsic localized modes in a macro-mechanical cantilever array with tunable on-site nonlinearity, Proc. IUTAM **5**, 288 (2012).

[16] M. Kimura and T. Hikihara, Coupled cantilever array with tunable on-site nonlinearity and observation of localized oscillations, Phys. Lett. A **373**, 1257 (2009).

[17] L. Yakusevich, *Nonlinear Physics of DNA* (Wiley-Interscience, New York, 1998).

[18] M. Peyrard, Nonlinear dynamics and statistical physics of DNA, Nonlinearity **17**, R1 (2004).

[19] M. Joyeux and A.-M. Florescu, Dynamical versus statistical mesoscopic models for DNA denaturation, J. Phys.: Condens. Matter **21**, 034101 (2009).

[20] M. Joyeux and S. Buyukdagli, Dynamical model based on finite stacking enthalpies for homogeneous and inhomogeneous DNA thermal denaturation, Phys. Rev. E **72**, 051902 (2005).

[21] D. Toko, C. B. Tabi, A. Mohamadou, and T. C. Kofane, Coherent modes and parameter selection in DNA models with finite stacking enthalpy, J. Comput. Theor. Nanosci. **9**, 97 (2012).

[22] A. Mvogo and T. C. Kofané, Fractional formalism to DNA chain and impact of the fractional order on breather dynamics, Chaos Interdisc. J. Nonlin. Sci. **26**, 123120 (2016).

[23] P. B. Ndjoko, J. M. Bilbault, S. Binczak, and T. C. Kofane, Compact-envelope bright solitary wave in a DNA double strand, Phys. Rev. E **85**, 011916 (2012).

[24] C. L. Gninzanlong, F. T. Ndjomatchoua, and C. Tchawoua, Discrete breathers dynamic in a model for DNA chain with a finite stacking enthalpy, Chaos **28**, 043105 (2018).

[25] X. Yang, X. Zhao, K. Yang, Y. Liu, Y. Liu, W. Fu, and Y. Luo, Biomedical applications of terahertz spectroscopy and imaging, Trends Biotechnol. **34**, 810 (2016).

[26] G. J. Wilmink and J. E. Grundt, Invited review article: Current state of research on biological effects of terahertz radiation, J. Infr. Millim. Terahertz Waves **32**, 1074 (2011).

[27] R. Shiurba, T. Hirabayashi, M. Masuda, A. Kawamura, Y. Komoike, W. Klitz, K. Kinowaki, T. Funatsu, S. Kondo, S. Kiyokawa, T. Sugai, K. Kawamura, H. Namiki, and T. Higashinakagawa, Cellular responses of the ciliate, Tetrahymena thermophila, to far infrared irradiation, Photochem. Photobiol. Sci. **5**, 799 (2006).

[28] J. Bock, Y. Fukuyo, S. Kang, M. L. Phipps, L. B. Alexandrov, K. Ø. Rasmussen, A. R. Bishop, E. D. Rosen, J. S. Martinez, H.-T. Chen, G. Rodriguez, B. S. Alexandrov, and A. Usheva, Mammalian stem cells reprogramming in response to terahertz radiation, PLoS One **5**, e15806 (2010).

[29] B. S. Alexandrov, V. Gelev, A. R. Bishop, A. Usheva, and K. Ø. Rasmussen, DNA breathing dynamics in the presence of a terahertz field, Phys. Lett. A **374**, 1214 (2010).

[30] P. Maniadis, B. S. Alexandrov, A. R. Bishop, and K. Ø. Rasmussen, Feigenbaum cascade of discrete breathers in a model of DNA, Phys. Rev. E **83**, 011904 (2011).

[31] A. Sulaiman, F. P. Zen, H. Alatas, and L. T. Handoko, Dynamics of DNA breathing in the Peyrard-Bishop model with damping and external force, Phys. D **241**, 1640 (2012).

[32] E. S. Swanson, Modeling DNA response to terahertz radiation, Phys. Rev. E **83**, 040901(R) (2011).

[33] P. Rosenau and J. M. Hyman, Compactons: Solitons with Finite Wavelength, Phys. Rev. Lett. **70**, 564 (1993).

[34] P. Maniadis and T. Bountis, Quasiperiodic and chaotic discrete breathers in a parametrically driven system without linear dispersion, Phys. Rev. E **73**, 046211 (2006).

[35] Y. S. Kivshar, Intrinsic localized modes as solitons with a compact support, Phys. Rev. E **48**, R43 (1993).

[36] A. V. Gorbach and S. Flach, Compactlike discrete breathers in systems with nonlinear and nonlocal dispersive terms, Phys. Rev. E **72**, 056607 (2005).

[37] S. Flach, Conditions on the existence of localized excitations in nonlinear discrete systems, Phys. Rev. E **50**, 3134 (1994).

[38] G. M. Chechin, G. S. Dzhelauhova, and E. A. Mehonoshina, Quasibreathers as a generalization of the concept of discrete breathers, Phys. Rev. E **74**, 036608 (2006).

[39] T. Bountis, T. Manos, and H. Christodoulidi, Application of the GALI method to localization dynamics in nonlinear systems, J. Comput. Appl. Math. **227**, 17 (2009).

[40] V. Marinca and N. Herisanu, *Nonlinear Dynamical Systems in Engineering* (Springer, Berlin, 2011).

[41] S. Wiggins, *Introduction to Applied Nonlinear Dynamical Systems and Chaos* (Springer-Verlag, New York, 2003).

[42] J. Pan, W. Chen, F. Tao, and W. Xu, Influence of impurities on solitons in the nonlinear LC transmission line, Phys. Rev. E **83**, 016601 (2011).

[43] N. V. Alexeeva, I. V. Barashenkov, and G. P. Tsironis, Impurity-Induced Stabilization of Solitons in Arrays of Parametrically Driven Nonlinear Oscillators, Phys. Rev. Lett. **84**, 3053 (2000).

[44] W. Chen, L. Lu, and Y. Zhu, Influence of impurities on hydrodynamic solitons, Phys. Rev. E **71**, 036622 (2005).

[45] T. Dauxois, M. Peyrard, and C. R. Willis, Discreteness effects on the formation and propagation of breathers in nonlinear Klein-Gordon equations, Phys. Rev. E **48**, 4768 (1993).

[46] K. Forinash, A. R. Bishop, and P. S. Lomdahl, Nonlinear dynamics in a double-chain model of DNA, Phys. Rev. B **43**, 10743 (1991).

[47] P. V. Larsen, P. L. Christiansen, O. Bang, J. F. R. Archilla, and Y. B. Gaididei, Energy funneling in a bent chain of Morse oscillators with long-range coupling, Phys. Rev. E **69**, 026603 (2004).

[48] M. Hisakado, Breather trapping mechanism in piecewise homogeneous DNA, Phys. Lett. A **227**, 87 (1997).

[49] F. Palmero, J. F. R. Archilla, D. Hennig, and F. R. Romero, Effect of base-pair inhomogeneities on charge transport along the DNA molecule, mediated by twist and radial polarons, New J. Phys. **6**, 13 (2004).

[50] M. Vanitha and M. Daniel, Internal nonlinear dynamics of a short lattice DNA model in terms of propagating kink-antikink solitons, Phys. Rev. E **85**, 041911 (2012).

[51] J. Cuevas, F. Palmero, J. F. R. Archilla, and F. R. Romero, Moving discrete breathers in a Klein-Gordon chain with an impurity, J. Phys. A **35**, 10519 (2002).

[52] A. Alvarez, F. R. Romero, J. F. R. Archilla, J. Cuevas, and P. V. Larsen, Breather trapping and breather transmission in a DNA model with an interface, Eur. Phys. J. B **51**, 119 (2006).

[53] J. J.-L. Ting and M. Peyrard, Effective breather trapping mechanism for DNA transcription, Phys. Rev. E **53**, 1011 (1996).

[54] T. Dauxois, M. Peyrard, and A. R. Bishop, Entropy-driven DNA denaturation, Phys. Rev. E **47**, R44 (1993).

[55] L. Brillouin, *Periodic Structure: Electronic Filters and Crystal Lattices* (McGraw-Hill, New York, 1946).

[56] J. L. Marín and S. Aubry, Breathers in nonlinear lattices: Numerical calculation from the anticontinuous limit, Nonlinearity **9**, 1501 (1996).

[57] D. K. Campbell, Nature **432**, 455 (2004).

[58] M. Weiss, T. Kottos, and T. Geisel, Taming chaos by impurities in two-dimensional oscillator arrays, Phys. Rev. E **63**, 056211 (2001).

[59] A. Gavrielides, T. Kottos, V. Kovanis, and G. P. Tsironis, Spatiotemporal organization of coupled nonlinear pendula through impurities, Phys. Rev. E **58**, 5529 (1998).

[60] T. Ikeda, Y. Harata, and K. Nishimura, Intrinsic localized modes of harmonic oscillations in pendulum arrays subjected to horizontal excitation, J. Comput. Nonlin. Dyn. **10**, 021007 (2015).

[61] T. Ikeda, Y. Harata, and K. Nishimura, Intrinsic localized modes of harmonic oscillations in nonlinear oscillator arrays, J. Comput. Nonlin. Dyn. **8**, 041009 (2013).

[62] T. Ikeda, Y. Harata, and R. Hiraoka, Intrinsic localized modes of 1/2-order subharmonic oscillations in nonlinear oscillator arrays, Nonlin. Dyn. **81**, 1759 (2015).

[63] M. E. King and A. F. Vakakis, A very complicated structure of resonances in a nonlinear system with cyclic symmetry: Nonlinear forced localization, Nonlin. Dyn. **7**, 85 (1995).

[64] S. Gutschmidt and O. Gottlieb, Nonlinear dynamic behavior of a microbeam array subject to parametric actuation at low, medium and large DC-voltages, Nonlin. Dyn. **67**, 1 (2012).

[65] A. J. Dick, B. Balachandran, and C. D. Mote, Intrinsic localized modes in microresonator arrays and their relationship to nonlinear vibration modes, Nonlin. Dyn. **54**, 13 (2008).

[66] D. Bitar, N. Kacem, N. Bouhaddi, and M. Collet, Collective dynamics of periodic nonlinear oscillators under simultaneous parametric and external excitations, Nonlin. Dyn. **82**, 749 (2015).

[67] M. Sato, T. Nakaguchi, T. Ishikawa, S. Shige, Y. Soga, Y. Doi, and A. J. Sievers, Supertransmission channel for an intrinsic localized mode in a one-dimensional nonlinear physical lattice, Chaos Interdisc. J. Nonlin. Sci. **25**, 103122 (2015).